Electronic properties of nanoentities revealed by electrically driven rotation

D. L. Fan[a,1], Frank Q. Zhu[b], Xiaobin Xu[a], Robert C. Cammarata[c], and C. L. Chien[c,d,1]

[a]Materials Science and Engineering Program, Texas Materials Institute, and Department of Mechanical Engineering, University of Texas at Austin, Austin, TX 78712; [b]Hitachi Global Storage Technologies, San Jose, CA 95135; [c]Department of Materials Science and Engineering, The Johns Hopkins University, Baltimore, MD 21218; and [d]Department of Physics and Astronomy, The Johns Hopkins University, Baltimore, MD 21218

Edited by Paul L. McEuen, Cornell University, Ithaca, NY, and approved April 20, 2012 (received for review January 9, 2012)

Direct electric measurement via small contacting pads on individual quasi-one-dimensional nanoentities, such as nanowires and carbon nanotubes, are usually required to access its electronic properties. We show in this work that 1D nanoentities in suspension can be driven to rotation by AC electric fields. The chirality of the resultantrotation unambiguously reveals whether the nanoentities are metal, semiconductor, or insulator due to the dependence of the Clausius–Mossotti factor on the material conductivity and frequency. This contactless method provides rapid and parallel identification of the electrical characteristics of 1D nanoentities.

electric tweezers | nanoparticles | manipulation

Quasi 1D entities, such as carbon nanotubes and various nanowires (e.g., metallic Au, ferromagnetic Co, semiconducting ZnO, and insulating SiO_2), have been intensely explored in recent years owing to their remarkable properties. Particularly fascinating are carbon nanotubes (CNTs), which may be multiwall carbon nanotubes (MWCNTs) and single-wall carbon nanotubes (SWCNTs) with greatly different properties. Even among SWCNTs, they can be metallic or semiconducting depending on the manner with which the graphene sheet rolls into the cylindrical shape (1). In fact, during synthesis of CNTs, both MWCNTs and SWCNTs, either metallic or semiconducting, are indiscriminately produced (2). To access the electronic properties of 1D entities, one usually resorts to direct electrical measurements of a single entity via metallic contact pads painstakingly patterned by lithography (1). The task becomes daunting when there are a variety of entities.

Freestanding nanoentities are typically suspended in a liquid to avoid adhesion to dry surfaces via the van der Waals forces. However, driven motion of suspended nanoentities is well known to be challenging because of the extremely low Reynolds number of 10^{-5} where viscous force overwhelms. Nevertheless, it has recently been shown in a scheme termed "electric tweezers" that suspended quasi-1D objects, including CNTs and nanowires, can be compelled to execute translational and rotational motion with precision by DC and AC electric fields applied to patterned electrodes (3–6). In particular, a suitably administered AC electric field can rotate the suspended 1D entities (7), where the rotation speed, chirality and rotation angle can be precisely controlled by the strength and duration of the applied electric fields.

In this work, we show that such electrically driven rotational motion can also reveal the electronic properties of the nanoentities. The chirality of the resultant rotation unambiguously reveals whether the nanoentities are metal, semiconductor, or insulator due to the dependence of the Clausius–Mossotti factor on the material conductivity and frequency. From the rotational characteristics, the imaginary part of the Clausius–Mossotti factor $\mathrm{Im}(K)$, a key electronic property of the nanoentities, can be determined solely from their rotational motion. We have thus demonstrated contactless probing of the electronic properties of 1D entities, providing a rapid, parallel, and nondestructive measurement of their electrical properties *without* any direct electrical contacts.

Results and Discussion

We illustrate this method using a variety of 1D entities from metallic to insulating, including MWCNTs, Au nanowires, ZnO nanowires, and SiO_2 nanotubes. All 1D entities except the MWCNTs (Alfar Aesar) have been synthesized by us with radii (r) in the 150 nm range, whereas MWCNTs have a small r of approximately 15 nm. All 1D entities have lengths (l) in the range of 3 to 10 μm, chosen for the ease of observation of their rotational motion by an optical microscope. These nanoentities were first suspended in deionized (DI) water, sonicated vigorously for 30 s before diluted to a solution of concentration of about 10^7/mL. A droplet (2 to approximately 10 μL in volume) was placed at the center of a quadruple electrode (consisting of two sets of parallel electrodes) and settled for 20 s before applying four 90° phase-shifted AC voltages (Fig. 1*A*). This arrangement provides a uniform rotating electric field with a specific magnitude and a frequency that can be controlled from 5 kHz to 1 MHz.

A quasi-1D entity suspended in a liquid of permittivity ε_m rotates due to the torque $\boldsymbol{T_e}$ as a result of a rotating electric field $\boldsymbol{E}$ with a magnitude of (8)

$$|\boldsymbol{T_e}| = |\boldsymbol{p} \times \boldsymbol{E}| = \frac{2\pi}{3} r^2 l \varepsilon_m \mathrm{Im}(K) E^2 \qquad [1]$$

where $\boldsymbol{p}$ is the induced dipole moment of a nanowire of radius r, length l, and $\mathrm{Im}(K)$ is the imaginary part of the Clausius–Mossotti factor K.

We rotated nanotubes from low speeds to higher speeds by increasing the applied voltage V, using a CCD camera of 30 frames/s to capture the rotational motion. At low rotation speeds, the orientation of the nanoentities as well as the rotational characteristics can be readily and accurately determined. The rotation of a MWCNT by the AC $\boldsymbol{E}$ field is shown as the overlapped snapshots (Fig. 1*G*) every 1/15 s (Fig. 1 *B–F*) and in Movie S1. The rotation angle increases linearly with time for a fixed voltage (Fig. 1*H*), due to the well-known consequence of motion in the extremely low Reynolds regime, where the viscous torque T_η from the drag force instantly balances the electric torque T_e^7. In particular, with increasing voltages, the rotational speed ω increases with V^2 as shown in Fig. 1*I*, which agrees with previous report (7). The linear dependence of ω versus V^2 observed in this work also agrees with Eq. **1**. Therefore, using our method and CCD camera, we can accurately characterize rotation of nanotubes/nanowires. Note that, to avoid possible

Author contributions: D.L.F. and C.L.C. designed research; D.L.F., F.Q.Z., and X.X. performed research; D.L.F. contributed new reagents/analytic tools; D.L.F., R.C.C., and C.L.C. analyzed data; and D.L.F., F.Q.Z., R.C.C., and C.L.C. wrote the paper.

The authors declare no conflict of interest.

This article is a PNAS Direct Submission.

[1]To whom correspondence may be addressed. E-mail: clc@pha.jhu.edu or dfan@austin.utexas.edu.

This article contains supporting information online at www.pnas.org/lookup/suppl/doi:10.1073/pnas.1200342109/-/DCSupplemental.

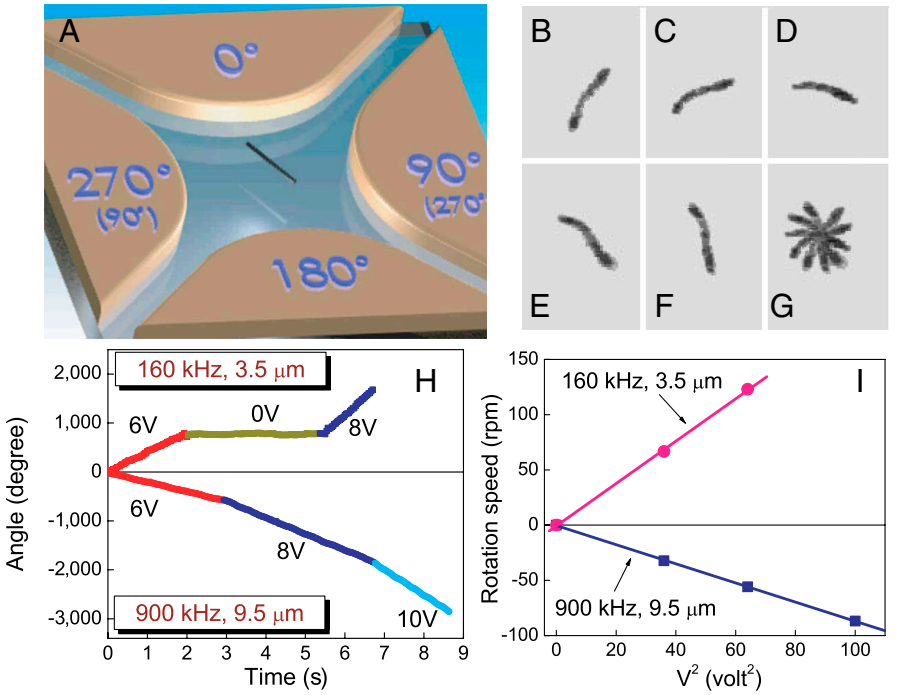

Fig. 1. (*A*) Schematic shows the rotation of multiwall carbon nanotubes (MWCNT) at the center of a quadruple electrode where four AC voltages applied to four electrodes with sequential 90° phase shift. (*B–F*) Snapshots of a rotating MWCNT every 1/15 s with the overlapped images shown in *G*. MWCNT can be rotated following or counter the ***E*** field. (*H*) In both cases, the rotation speeds are uniform at a fixed voltage, whereas the angle increases linearly with time, and (*I*) and the speed increases with V^2.

ambiguity in imaging analysis, we only analyze the rotation with speeds of less than 900 rpm, above which we use a high-speed CCD camera operating at 2,000 frames/s. The observation of rotation is free of stroboscopic artifacts.

For quasi-1D nanoentities, the viscous torque T_η can be approximated as (9)

$$T_\eta \approx \frac{\pi}{3} l^3 \eta \Omega C, \qquad [2]$$

where Ω is the rotation speed of the entity, η the viscosity, and C is approximately a constant for a rod shaped entities of a fixed length. The value of $\mathrm{Im}(K)$ can be readily obtained from $T_\mathrm{E} + T_\eta = 0$,

$$\mathrm{Im}(K) = -\frac{1}{2}\frac{\eta l^2 \Omega C}{\varepsilon_m r^2 E^2}, \qquad [3]$$

showing that the Clausius–Mossotti factor $\mathrm{Im}(K)$, which is an intrinsic electronic characteristic of the quasi-1D entity, can be measured from its rotation speed Ω as a result of the rotating electric field. Furthermore, the rotation chirality is the same or opposite to the rotation direction of the ***E*** field, if $\mathrm{Im}(K)$ should be negative and positive respectively. These characteristics have indeed been experimentally observed.

We have measured the rotation speed (expressed as Ω/V^2) of the MWCNT in ***E*** field at a frequency ω from 20 kHz to 1 MHz as plotted in Fig. 2*A*. For a 9.5 μm long MWCNT, rotation direction initially has the same chirality as that of the AC ***E*** field, and rotation speed increases with the AC frequency to about 200 kHz. Then rotation starts to slow down upon at higher frequency and eventually stops ($\Omega = 0$) at 544 kHz. Above 544 kHz, MWCNT rotates with an opposite chirality. We have observed similar results for MWCNTs with other lengths from 3.5 to 7.2 μm. We define the frequency with no rotation as the crossover frequency, which evidently depends also on the length of the MWCNT (Fig. 2*A*).

Using Eq. **3**, we have calculated the values of $\mathrm{Im}(K)$ and plotted in Fig. 2*B* as a function of AC frequency. The results in Fig. 2 *A* and *B*, apart from a minus sign, are similar in shape.

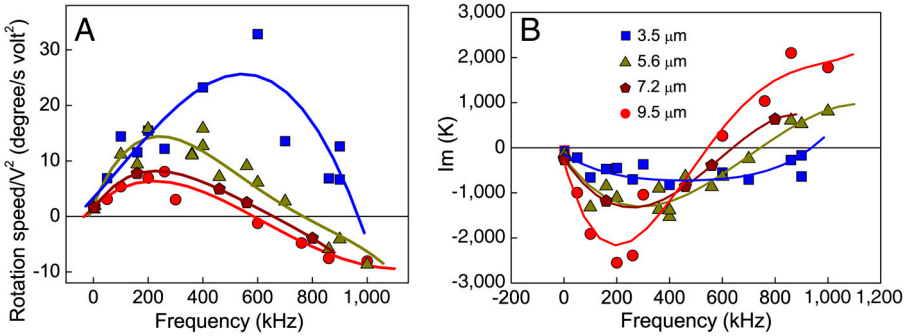

Fig. 2. (*A*) Normalized rotation speed versus AC frequency for MWCNT with length of 3.5 (squares), 5.6 (triangles), 7.2 (pentagons), and 9.5 μm (circles). The rotation is in the same (at low frequency) and opposite (at high frequency) direction with ***E*** field. The peak frequency shifts lower with increasing aspect ratio of MWCNT. (*B*) Derived $\mathrm{Im}(K)$ of MWCNT with close relation with rotation shown in *A*. The peak value $|\mathrm{Im}(K)_{\max}|$ decreases with decreasing aspect ratio.

However, the larger peak in rotation speed Ω occurs at the shorter MWCNT, whereas the larger peak in $|\mathrm{Im}(K)_{\max}|$ occurs at the longer MWCNT. These experimental results are consistent to Eq. **3**, which prescribes that $\mathrm{Im}(K)$ be proportional to $-l^2$ Ω. Consequently, the rotation speed Ω reveals both the electronic factor $\mathrm{Im}(K)$ and the physical length l of the 1D entities.

To quantitatively extract the values of the electronic properties of 1D entities, we have modeled the 1D entities as elongated ellipsoids, for which the Clausius–Mossotti factor K can be expressed by (8, 10)

$$K = \frac{\varepsilon_p^* - \varepsilon_m^*}{\varepsilon_m^* + L(\varepsilon_p^* - \varepsilon_m^*)}, \qquad [4]$$

where $\varepsilon_p^* = \varepsilon_p - i\sigma_p/\omega$ and $\varepsilon_m^* = \varepsilon_m - i\sigma_m/\omega$ are the complex permittivity of the particle and medium respectively involving the permittivity (ε_p and ε_m) and the conductivity (σ_p and σ_m) of the nanoentity and the medium, and the frequency ω of the rotating AC electric field. Since the applied AC $\boldsymbol{E}$ field has a much higher frequency than that of the mechanical rotation, the depolarization factor L is effectively a constant dictated by the aspect ratio of the 1D entity (11). Then the imaginary part of the Clausius–Mossotti factor K can be obtained from Eq. **4** in a straightforward manner as

$$\mathrm{Im}(K) = \frac{\varepsilon_p\sigma_m - \varepsilon_m\sigma_p}{\omega[(\varepsilon_m + L\varepsilon_p - L\varepsilon_m)^2 + \frac{1}{\omega^2}(\sigma_m + L\sigma_p - L\sigma_m)^2]}. \qquad [5]$$

Because the denominator is always positive, the numerator $\varepsilon_p\sigma_m - \varepsilon_m\sigma_p$ dictates the sign of $\mathrm{Im}(K)$. Since $\frac{\varepsilon}{\sigma}$ is the charge relaxation time τ, thus $\mathrm{Im}(K) \propto (\tau_p - \tau_m)$, i.e., the sign of $\mathrm{Im}(K)$ as well as the chirality of the rotation depends on the relative values of τ_p and τ_m. This is illustrated experimentally in Fig. 3*A* for a MWCNT of 9.5 μm length at a frequency below and above the frequency 544 kHz when the charge relaxation time of MWCNT is respectively shorter and longer than that of DI water. At 544 kHz, $\tau_p = \tau_m$, $\mathrm{Im}(K) = 0$, the MWCNT ceases to rotate. As a result, from $\tau_p = \tau_m = \frac{\varepsilon_p}{\sigma_p} = \frac{\varepsilon_m}{\sigma_m}$ at 544 kHz, the value of the ratio ε_p/σ_p of the MWCNT has the same value of ε_m/σ_m of the medium.

We next address the peak position, which increases to higher frequencies with the decrease of the length of the MWCNTs as shown in Fig. 2*B*. From Eq. **5**, the peak position of $\mathrm{Im}(K)$ occurs at ω_p with the value of

$$\omega_p = \frac{\sigma_m + L\sigma_p - L\sigma_m}{\varepsilon_m + L\varepsilon_p - L\varepsilon_m}. \qquad [6]$$

The effective depolarization factor L can be approximated as (12) $L \approx (\ln\frac{l}{r} - 1)/(\frac{l}{2r})^2$. Since $l \gg r$ and hence $L \ll 1$ and for conducting entities $\sigma_p \gg \sigma_m$, we have $\sigma_p \approx (\omega_p\varepsilon_m - \sigma_m)/L$ from Eq. **6**. Thus, with the values of σ_m and ε_m of the medium, the frequency ω_p at which $\mathrm{Im}(K)$ peaks, the value of L dictated by the dimensions l and r of the 1D entities, the rotational motion allows one to determine the conductivity σ_p of the 1D entities via $\sigma_p \approx (\omega_p\varepsilon_m - \sigma_m)/L$, for any actual electrical measurements. In Fig. 3*B*, we show the conductivity σ_p so determined as a function of length l of the MWCNT. Very interestingly, we have found σ_p to increase linearly with the length l, i.e.,$\sigma_p \propto l$. For MWCNT of approximately the same cross-section, this means that the MWCNT has a constant resistance of 8.7×10^8 Ω, *regardless* of length. This is the hallmark of ballistic electron transport, which has been theoretically predicted (13–15). Our work is one of the few that indicate ballistic nature of electron transport in MWCNT (16–18).

We note that the resistance of 8.7×10^8 Ω is higher than most values reported from electrical contact measurements in the range of 10^5 to 10^7 Ω (19–21). This may be the result of both theoretical simplifications and experimental differences. The theoretical expression of $\mathrm{Im}(K)$ as described in Eq. **5** assumes a MWCNT as a solid ellipsoid with a constant effective depolarization factor L. In reality, the nature of materials inside the tubular structure of a MWCNT is more complex. Experimentally, only the outermost shell of the MWCNT is electrically contacted and measured (15–19). The materials inside the shell also contribute significantly but in a poorly specified manner. In contrast, our method determines the electronic properties of a MWCNT from its mechanical motion in an $\boldsymbol{E}$ field without using electrical contacts. The electrical resistance so obtained is not mainly from the outermost shell but the response of the entire MWCNT to the external electric field. Theoretical calculations shows that the MWCNTs of larger diameters (>10 nm) are more metallic (lower resistance) than those of smaller diameters (higher resistance) (22) and in SWCNT the resistance reaches the range of 10^8–10^9 Ω (21).Therefore, it can be reasonably understood that the measured resistance using our electromechanical approach is higher due to the overall response from all the shells in the MWCNTs than those by the electrical-contact method.

In addition to MWCNT, we have also used the same method to successfully rotate metallic nanowires such as Au (radius $r \approx 150$ nm, length $l = 3.5 \pm 0.3$ μm), Pt ($r \approx 150$ nm, $l = 3.3 \pm 0.2$ μm), semiconducting nanowires of ZnO ($r \approx 150$ nm, $l \approx 3.3$ and 3.8 μm), and insulating SiO_2 nanotubes ($r_{\mathrm{inner}} \approx 150$ nm, shell thickness 300 nm, $l \approx 8.7$ μm). For metallic nanowires, the nanowires rotate with the same chirality with $\boldsymbol{E}$ field from 5 kHz to 1 MHz as in Fig. 4*A* because the charge relaxation time (τ_p) is much shorter than τ_m of the DI water due to the high conductivity of the metallic nanowires (Movie S2). For the semiconducting nanowires, the behavior is different. The nanowires rotate with the same chirality as that of the $\boldsymbol{E}$ field at low frequencies, but with opposite chirality at high frequencies. At low frequencies, similar to metallic nanowires, the charge relaxation times (τ_p)

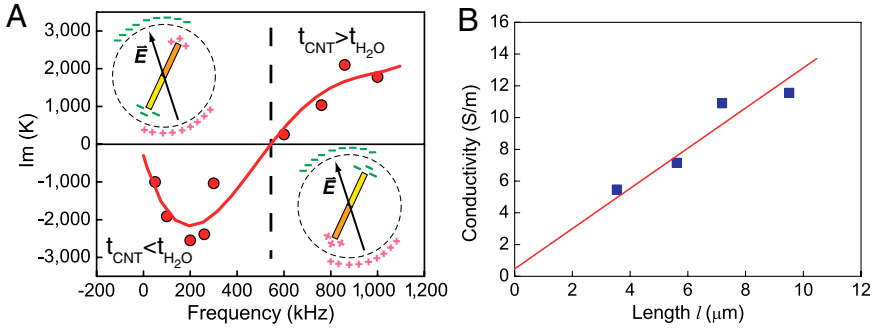

Fig. 3. (*A*) Depending on the charge relaxation time τ_{CNT} of the MWCNT relative to τ_{water} of DI water, MWCNT rotates following the $\boldsymbol{E}$ field when $\tau_{\mathrm{CNT}} < \tau_{\mathrm{water}}$ and $Im(K) < 0$, opposite to the $\boldsymbol{E}$ field when $\tau_{\mathrm{CNT}} > \tau_{\mathrm{water}}$ and $\mathrm{Im}(K) > 0$, and will not rotate when $\tau_{\mathrm{CNT}} = \tau_{\mathrm{water}}$ and $\mathrm{Im}(K) = 0$. (*B*) The conductivity of MWCNT calculated from $\mathrm{Im}(K)$ increases linearly with the length, indicating the ballistic transport characteristic of MWCNT.

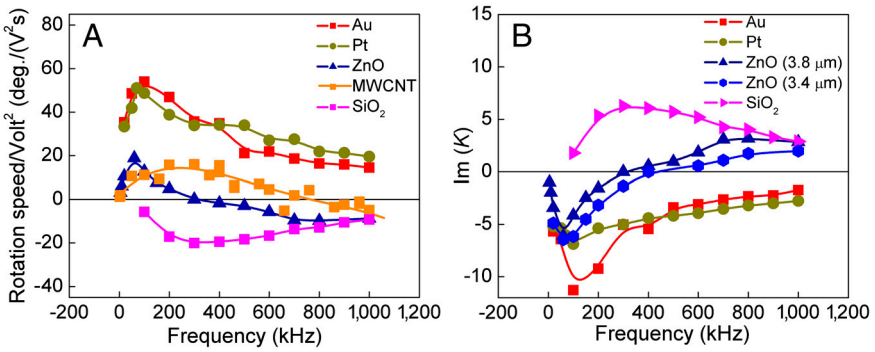

Fig. 4. (*A*) Rotation of metallic (Au, Pt), semiconducting (ZnO) nanowires, insulating (SiO_2) nanotubes, and MWCNT. The rotation of metallic nanowires follows same chirality as ***E*** field from 0.05 to approximately 1 MHz, whereas semiconducting nanowires switch chirality at high frequencies. Insulating nanotubes always rotate counter to the ***E*** field in the same frequency range. It demonstrates a contactless and nondestructive method to determine the metallicity of nanowires. (*B*) The $\mathrm{Im}(K)$ as function of frequency of metallic (Au, Pt), semiconducting nanowires (ZnO), and insulating (SiO_2) nanotubes.

of the semiconducting nanowires are shorter than that of DI water. At high frequencies, however, due to the lower conductivity of semiconducting nanowires, the charge relaxation time is longer than that of DI water and hence rotation chirality reverses. These features have been observed in ZnO nanowires, where the rotation reverses chirality at 300 kHz for ZnO as shown in Fig. 4*A*. Movie S3 shows the switching of the rotation chirality of ZnO nanowires when the AC frequency changed from 50 to 700 kHz. For insulating nanowires/nanotubes such as SiO_2, the rotation always counter to the ***E*** field direction, because the charge relaxation time (τ_p) is much longer than τ_m of the DI water due to the low conductivity of the insulating nanowires/nanotubes as shown in Movie S4. As a result, the rotation of mixed Au nanowires and SiO_2 nanotubes, is always opposite to each other at both low and high frequencies. We can therefore distinguish between metallic, semiconducting, and even insulating nanoentities by their rotation chirality.

From the rotation characteristics, we can calculate $\mathrm{Im}(K)$ as a function of frequency as shown in Fig. 4*B*. $\mathrm{Im}(K)$ of Au and Pt nanowires are negative from 20 KHz to 1 MHz, with peak values at around 100 kHz; Au exhibits a higher peak than Pt due to its higher conductivity. On the other hand, $\mathrm{Im}(K)$ of SiO_2 nanotubes are always positive in the same frequency range. $\mathrm{Im}(K)$ of wide band-gap semiconducting ZnO nanowires exhibits a negative peak, changes signs and becomes positive at high frequencies (Fig. 4*B*). We also noticed that the $\mathrm{Im}(K)$ MWCNTs in Fig. 2*B* shows similarity with semiconducting nanowires where $\mathrm{Im}(K)$ changes sign at a few hundred kHz. This again can be understood by the fact that our method is a result of the overall electrical properties of MWCNTs. Even though, most electric-contact measurement on the outermost shells of MWCNTs shows that MWCNTs with large diameters are metallic (e.g., 30 nm in diameter) (21), the inner shells, especially those with small diameters (<10 nm), prone to be semiconducting, and their electric properties have been reflected in our measurements.

These results show that by rotating quasi-1D entities in suspension by AC electric field, we can readily identify them as being metallic, semiconducting, or insulating. From the dependence of rotation speed on frequency, we can measure the frequency dependence of $\mathrm{Im}(K)$, and the cross-over frequency measures the relaxation time of the entities, relative to the medium in which the 1D entities are suspended. This contactless and nondestructive method can be performed in parallel involving many 1D entities.

In summary, we have demonstrated a contactless, nondestructive, and parallel method to determine the electronic properties of 1D entities from their electrically driven rotational motion. These entities include MWCNT, nanowires, and nanotubes, with electrical characteristics that are metallic, semiconducting or insulating. We found evidences that MWCNTs are ballistic conductors with a constant length-independent resistance.

Materials and Methods

Various metallic nanowires such as Au, Pt, and Ag nanowires were fabricated by using electrodeposition in nanoporous templates as shown in Fig. S1*A* (6). In a three-electrode setup, a sputtered Cu layer at the back of the nanoporous template serves as a working electrode, a Pt mesh serves as a counter electrode, and a Ag/AgCl electrode serves as the reference electrode. Au and Ag nanowires were electrodeposited from commercial electrolytes of 434 HS RTU and 1006 Silver (Technic, Inc.), respectively, at a voltage of −1 to −0.09 V (Ag/AgCl reference). Pt was electrodeposited from a solution of at −0.45 V (Ag/AgCl reference). The growth of the nanowires commences at the bottom of nanopores at the working electrode. The amount of electric charge passing through the circuit controls the length of the nanowires (or of the segments of a nanowire). The pore sizes of the template control the diameters of the nanowires from 20 to 400 nm. The nanowires deposited inside the nanoporous templates were released in suspension by dissolution of the template in 2 M sodium hydroxide, followed by centrifuging and dispersion in deionized water and ethanol, each for two times, before resuspended in DI water.

SiO_2 nanotubes were synthesized by using electrodeposited Ag nanowires as templates. We first coated amorphous silicon dioxide (SiO_2) on the surface of the Ag nanowires. The reaction took place in tetraethyl orthosilicate (TEOS) solution for 2–5 h via which the thickness of the SiO_2 can be precisely controlled from a few nanometers to 1 μm. When the SiO_2 nanoshells have been successfully formed around the Ag nanowires, we selectively etched the Ag to obtain the SiO_2 nanotubes with a mixture (4:1:1) of methanol (99%): hydrogen peroxide (30%):ammonia hydroxide (28% to approximately 30% as NH_3), as shown in Fig. S1*B*.

ZnO nanowires were fabricated by a well established hydrothermal method as shown in Fig. S1*C* (3). Fourteen milliliters of 10 mM $Zn(NO_3)_2 \bullet 6H_2O$ (Zinc Nitrate Hexahydrate, Aldrich, 98%) and 14 mL of 10 mM $C_6H_{12}N_4$ (Hexamethylenetetramine, Aldrich, 99%) were mixed at room temperature and transferred to a 50 mL glass bottle and incubated at 90° C for 16 h before ZnO nanowires were collected from the bottom of the bottle, dispersed, and centrifuged by DI water for two times, and redispersed in DI water.

ACKNOWLEDGMENTS. This work has been supported in part by National Science Foundation (NSF) grant DMR05-20491. D.L.F. and X.X. gratefully acknowledge support from the Welch Foundation through Grant F-1734, National Institutes of Health Grant 1R41EB012885-01, and University of Texas at Austin Startup support. R.C.C. gratefully acknowledges support from NSF Grant DMR 0706178.

1. Dresselhaus MS, Dresselhaus G, Avouris P, Smalley RE (2001) *Carbon Nanotubes: Synthesis, Structure, Properties, and Applications* (Springer, Berlin), 1st Ed.
2. Fonseca A, et al. (1998) Synthesis of single- andmulti-wall carbon nanotubes over supported catalysts. *Appl Phys A Mater Sci Process* 67:11–22.
3. Fan DL, Cammarata RC, Chien CL (2008) Precision transport and assembling of nanowires in suspension by electric fields. *Appl Phys Lett* 92:093115.
4. Fan DL, Zhu FQ, Cammarata RC, Chien CL (2011) Electric tweezers. *Nano Today* 6:339–354.

5. Fan DL, et al. (2010) Sub-cellular resolution delivery of a cytokine via precisely manipulated nanowires. *Nat Nanotechnol* 5:545–551.
6. Fan DL, Zhu FQ, Cammarata RC, Chien CL (2004) Manipulation of nanowires by ac electric fields. *Appl Phys Lett* 85:4175–4177.
7. Fan DL, Zhu FQ, Cammarata RC, Chien CL (2005) Controllable high-speed rotation of metallic nanowires. *Phys Rev Lett* 94:247208.
8. Jones TB (1995) *Electromechanics of Particles* (Cambridge Univ Press, Cambridge, UK).
9. Keshoju K, Xing H, Sun L (2007) *Appl Phys Lett* 91:123114.
10. Miller RD, Jones TB (1993) Electro-orientation of ellipsoidal erythrocytes. *Biophys J* 64:1588–1595.
11. Pohl HA, Pethig R (1977) Dielectric measurements using non-uniform electric field (dielectrophoretic) effects. *J Phys E Sci Instrum* 10:190–192.
12. Asamia K, Yonezawa T (1995) Dielectric behavior of non-spherical cells in culture. *Biochim Biophys Acta* 1245:317–324.
13. Chico L, Benedict LX, Louie SG, Cohen ML (1996) Quantum conductance of carbon nanotubes with defects. *Phys Rev B* 54:2600–2606.
14. Tian W, Datta S (1994) Aharonov-Bohm-type effect in graphene tubules: A Landauer approach. *Phys Rev B* 49:5097–5100.
15. Lin MF, Shung KWK (1995) Magnetoconductance of carbon nanotubes. *Phys Rev B* 51:7592–7597.
16. Li HJ, Lu WG, Li JJ, Bai XD, Gu CZ (2005) Multichannel ballistic transport in multiwall carbon nanotubes. *Phys Rev Lett* 95:086601.
17. Frank S, Poncharal P, Wang ZL, de Heer WA (1998) Carbon nanotube quantum resistors. *Science* 280:1744–1746.
18. Urbina A, Echeverria I, Garrido AP, Sanchez AD, Abellan J (2003) Quantum conductance steps in solutions of multiwalled carbon nanotubes. *Phys Rev Lett* 90:106603.
19. Dai H, Wong E, Lieber CM (1996) Probing electrical transport in nanomaterials: conductivity of individual carbon nanotubes. *Science* 272:523–526.
20. Hobara R, et al. (2004) Electronic transport in multiwalled carbon nanotubes contacted with patterned electrodes. *Jpn J Appl Phys* 43:L1081–L1084.
21. Martel R, Schmidt T, Shea HR, Hertel T, Avouris PH (1998) Single- and multi-wall carbon nanotube field-effect transistors. *Appl Phys Lett* 73:2447–2449.
22. Dresselhaus MS, Dresselhaus G, Eklund PC (1996) *Science of fullerenes and carbon nanotubes* (Academic Press, San Diego, CA).